C78 Cage Isomerism Defined by Trimetallic Nitride Cluster Size: A Computational and Vibrational Spectroscopic Study

ARTICLE *in* THE JOURNAL OF PHYSICAL CHEMISTRY B · MAY 2007

Impact Factor: 3.3 · DOI: 10.1021/jp068661r · Source: PubMed

5 AUTHORS, INCLUDING:

Alexey A Popov
Leibniz Institute for Solid State and Materials…
188 PUBLICATIONS **3,412** CITATIONS
SEE PROFILE

Shangfeng Yang
University of Science and Technology of China
141 PUBLICATIONS **2,847** CITATIONS
SEE PROFILE

Joanna C. Wong
ETH Zurich
14 PUBLICATIONS **355** CITATIONS
SEE PROFILE

C_{78} Cage Isomerism Defined by Trimetallic Nitride Cluster Size: A Computational and Vibrational Spectroscopic Study

Alexey A. Popov,*,† Matthias Krause,‡,§ Shangfeng Yang,‡ Joanna Wong,‡ and Lothar Dunsch*,‡

Chemistry Department, Moscow State University, Moscow 119992, Russia, Group of Electrochemistry and Conducting Polymers, Leibniz-Institute for Solid State and Materials Research Dresden, D-01171 Dresden, Germany, and Institute of Ion Beam Physics and Materials Research, Forschungszentrum Dresden-Rossendorf, PF 510119, D-01314 Dresden, Germany

Received: December 17, 2006

Molecular structures of $Dy_3N@C_{78}$ and $Tm_3N@C_{78}$ clusterfullerenes are addressed by the IR and Raman vibrational spectroscopic studies and density functional theory (DFT) computations. First, extensive semiempirical calculations of 2927 isomers of C_{78} hexaanions followed by DFT optimization were applied to establish their relative stability. Then, DFT calculations of a series of $M_3N@C_{78}$ (M = Sc, Y, Lu, La) isomers were performed which have shown that the stability order of the isomers depends on the cluster size. While the Sc_3N cluster is planar in the earlier reported $Sc_3N@C_{78}$ (D_{3h}: 24 109) clusterfullerene, relatively large Y_3N and Lu_3N clusters would be forced to be pyramidal inside this cage, which would result in their destabilization. Instead, these clusters remain planar in the nonisolated pentagon rule (non-IPR) C_2: 22 010 isomer making $Y_3N@C_{78}$ and $Lu_3N@C_{78}$ clusterfullerenes with this cage structure the most stable ones. Finally, on the basis of a detailed analysis of their IR and Raman spectra supplemented with DFT vibrational calculations, the recently isolated $Tm_3N@C_{78}$ and the major isomer of $Dy_3N@C_{78}$ are assigned to the non-IPR C_2: 22 010 cage structure. A detailed assignment of their experimental and computed IR and Raman spectra is provided to support this conclusion and to exclude other cage isomers.

Introduction

An interesting peculiarity of the endohedral fullerenes, that is, fullerenes with atoms, ions, or clusters trapped in their inner space, is that the carbon cage isomerism is defined by the encapsulated species since structurally characterized cage isomers in endohedral fullerenes are usually different from those of the empty fullerenes.[1] This fact is so far understood by a formal transfer of several electrons from the encaged species to the lowest unoccupied molecular orbitals (LUMOs) of the fullerene.[1,2] Quantum-chemical calculations have shown that the stability order of the fullerene isomers obeying the isolated pentagon rule (IPR) may change upon charging the fullerene.[2] Isolation of the non-IPR $Sc_2@C_{66}$,[3a] $Sc_3N@C_{68}$,[4a] $La_2@C_{72}$,[3b] $Sc_2C_2@C_{68}$,[3c] and $La@C_{72}$[3d] and recent characterization of two new non-IPR trimetallic nitride clusterfullerenes, $Sc_3N@C_{70}$[4b] and $Tb_3N@C_{84}$,[4c] demonstrate that IPR itself may break down if the electrons are transferred from the encaged species to the fullerene. Hence, consideration of the cage structures for new endohedral fullerenes should not be limited to IPR cages only.

Trimetallic nitride clusterfullerenes of the general formula $M_3N@C_{2n}$, where M may be Sc, Y, or rare-earth metal, constitute a special family within the class of endohedral fullerenes because of the large highest occupied molecular orbital (HOMO)−LUMO gaps, enhanced stability, and appreciable yields which may be achieved in their production.[1b,5] Besides $Sc_3N@C_{80}$,[5a] $Sc_3N@C_{78}$,[5b] and $Sc_3N@C_{68}$[4a] reported earlier, a wealth of trimetallic nitride clusterfullerenes are isolated by now, including a set of $M_3N@C_{80}$ molecules (M = Y, Tb, Ho, Er, Lu),[5c,5d] $Tb_3N@C_{84}$,[4c] $Sc_3N@C_{70}$,[4b] and recently reported $Gd_3N@C_{2n}$ (n = 40−44),[6a] $Tm_3N@C_{2n}$ (n = 38−44),[6b] and $Dy_3N@C_{2n}$ (n = 38−49)[6c] families. X-ray crystallographic, vibrational, and UV−vis−NIR spectroscopic studies revealed that the most abundant clusterfullerenes are always based on the C_{80} (I_h: 7) cage isomer independent of the metal in the M_3N cluster.[5,6] However, upon lowering the cage size to C_{78}, the independence of the cage isomeric structure on the cluster is no longer valid. Up to now, four $M_3N@C_{78}$ clusterfullerenes were isolated (M = Sc,[5c] Tm,[6b] and two isomers of Dy[6c] referred hereafter as I and II). As established by X-ray crystallographic study,[5c] $Sc_3N@C_{78}$ has a cage structure of IPR-obeyed D_{3h}: 24 109 isomer (also referred to as isomer 5 when only IPR structures are considered[7]). X-ray or ^{13}C NMR data are not available yet for $Tm_3N@C_{78}$ and the two isomers of $Dy_3N@C_{78}$ because of the limited amounts available, but high-performance liquid chromatography (HPLC) elution behavior and spectroscopic properties (Figures 1 and 2) of these clusterfullerenes are quite different from those of $Sc_3N@C_{78}$, suggesting that other cage isomers should be considered. Using the (LUMO+2)−(LUMO+3) gap of the IPR fullerene cages as a criterion of their capability to form clusterfullerenes, Campanera et al.[8] have found that only the D_{3h}: 24 109 isomer of C_{78} is a suitable host for trimetallic nitride clusters. Hence, $Tm_3N@C_{78}$ and $Dy_3N@C_{78}$ most probably have non-IPR cages.

Because of the unique sensitivity of vibrational (IR and Raman) spectroscopy to molecular structure, its application can assist substantially in structure elucidation, especially when other

* To whom correspondence should be addressed. E-mail: popov@phys.chem.msu.ru (A. A. P.); L.Dunsch@ifw-dresden.de (L. D.).
† Moscow State University.
‡ Leibniz-Institute for Solid State and Materials Research Dresden.
§ Institute of Ion Beam Physics and Materials Research.

10.1021/jp068661r CCC: $37.00
Published on Web 03/14/2007

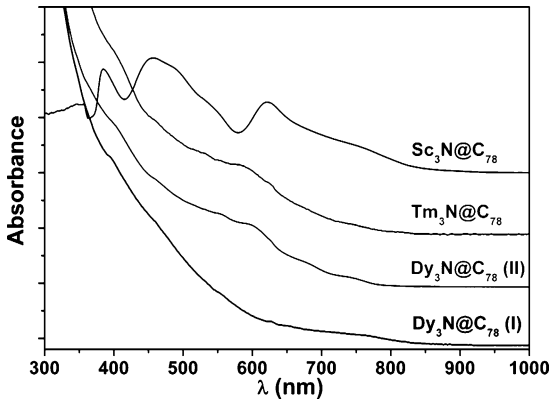

Figure 1. UV−vis−NIR absorptions spectra of $M_3N@C_{78}$ (M = Sc, Tm, Dy) dissolved in toluene.

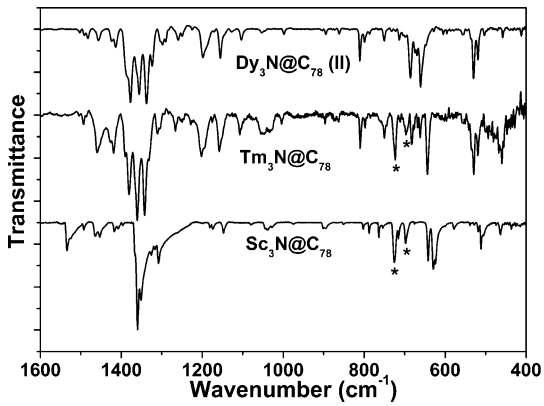

Figure 2. FTIR spectra of $M_3N@C_{78}$ (M = Sc, Tm, Dy). Asterisks denote toluene bands.

commonly used methods of structural analysis such as X-ray or NMR have failed to provide unambiguous answers, are not useful because of the low amount of the fullerene under study, or are unavailable. Nevertheless, until very recently, the application of vibrational spectroscopy in fullerene chemistry was very limited, suffering from the lack of a theoretical background because of low feasibility of the required first-principle vibrational calculations for molecules of such large size (n(C) > 60). Reported examples included mainly vibrational analysis of the highly symmetrical fullerenes C_{60},[9] C_{70},[10] and C_{84}[11] with the use of B3LYP/6-31G* approach or the use of less sophisticated (but less reliable) methods for azafullerene,[12] $C_{60}H_{36}$,[13] C_{60} polymers,[14] and some endohedral metallofullerenes.[15] The first-principle vibrational calculations, at least with 6-31G* or comparable basis sets, were hardly feasible for larger or low symmetrical systems. The increased computational demands were prohibitive for these molecules since in this case the interpretation of the spectra requires even more accurate prediction of vibrational frequencies and relative intensities than for highly symmetrical ones. Taking advantage of the density fitting technique[16] which allows considerable acceleration of pure density functional theory (DFT) computations, we have successfully applied the PBE[17]/TZ2P approach to interpret vibrational spectra of polymeric C_{60},[18] hydrofullerenes ($C_{60}H_{18}$, $C_{60}H_{36}$),[19] fullerene bromides ($C_{60}Br_6$, $C_{60}Br_8$, $C_{60}Br_{24}$, $C_{70}Br_{10}$),[20,21] chlorides ($C_{60}Cl_6$, $C_{60}Cl_{30}$),[22] and fluorides ($C_{60}F_{20}$, $C_{60}F_{36}$, $C_{60}F_{48}$).[23] The combination of experimental IR or Raman spectra with DFT-computed vibrational data enabled us to perform a detailed vibrational assignment for a set of fullerene derivatives, providing an unambiguous structural assignment for $C_{60}F_{20}$,[23a] $C_{60}F_{24}$,[23b] and $C_{60}F_{36}$,[23c] which could not be accomplished with the use of NMR data, and to distinguish two very similar isomers of $C_{60}F_{48}$[23c] otherwise undistinguishable even with the use of X-ray and NMR techniques. In the case of $C_{70}Br_{10}$, the agreement between the simulated IR spectrum of one of the isomers of $C_{70}Br_{10}$ molecule with the experimental IR data served as a basis for the first structural conjecture,[21a] which was confirmed by X-ray single-crystal structural data later on.[21b] Application of the PBE/TZ2P method was found to be advantageous in the field of the clusterfullerenes as well, being the basis for the complete assignment of IR and Raman spectra of $Sc_3N@C_{68}$ and $Sc_3N@C_{78}$,[24] aiding in the elucidation of the molecular structures of $Gd_xSc_{3-x}@C_{80}$ (I)[25] and $Sc_3N@C_{70}$,[4b] and establishing the extent of the cluster−cage interactions in the $M_3N@C_{80}$ (M = Sc, Y, Gd−Lu) clusterfullerenes.[26]

In this paper, we address the problem of the cage isomerism in $M_3N@C_{78}$ clusterfullerenes by in-depth quantum-chemical calculations and vibrational spectroscopic study. The most suitable cage isomers of $M_3N@C_{78}$ are established, and molecular structure of $Tm_3N@C_{78}$ and $Dy_3N@C_{78}$ (II) is proposed. The structural assignment for these clusterfullerenes is further supported by the analysis of their IR and Raman spectra.

Experimental and Computational Details

Synthesis and isolation of $Tm_3N@C_{78}$ and two isomers of $Dy_3N@C_{78}$ were reported earlier;[6b,6c] 500 μg of $Dy_3N@C_{78}$ (II) and 150 μg of $Tm_3N@C_{78}$ were isolated for spectroscopic studies. Isolated amounts of $Dy_3N@C_{78}$(I) were not sufficient for vibrational spectroscopic studies. UV−vis−NIR spectra of the clusterfullerenes dissolved in toluene were recorded on a UV−vis−NIR 3101-PC spectrometer (Shimadzu, Japan) of 1-nm resolution using a quartz cell of 1-mm layer thickness. For Fourier transform infrared (FTIR) and Raman measurements, clusterfullerenes dissolved in toluene (1 mL) were used to drop-coat KBr single-crystal disks. Residual solvent was removed by heating the polycrystalline films in a vacuum of $2\cdot10^{-6}$ mbar at 235 °C for 3 h. FTIR spectra were measured at room temperature in transmission mode by an IFS 66v spectrometer (Bruker, Germany) with a resolution of 2 cm^{-1}. Raman scattering was excited by the 647.1 nm and 515.4 nm emission lines of a Kr^+ and Ar^+ ion laser (Innova 300 series, Coherent, United States). The scattered light was collected in a 180° backscattering geometry and was analyzed by a T 64000 triple spectrometer (Jobin Yvon, France) whose spectral bandpass was set to 2 cm^{-1}. A rotation device was used as sample holder to exclude heat-induced sample changes in the Raman experiments.

Semiempirical calculations at the AM1[27] level were performed using PC GAMESS package.[28] DFT calculations were performed using PBE functional[17] and TZ2P-quality basis set with SBK-type effective core potential for Sc, Y, La, and Lu atoms implemented in the PRIRODA package.[16] The quantum-chemical code employed expansion of the electron density in an auxiliary basis set to accelerate the evaluation of the Coulomb and exchange-correlation terms. No symmetry constraints were adopted in the optimization, while location of the true energy minimum in each case was verified by Hessian computations. In the analysis of the spectra of $Dy_3N@C_{78}$ (II), the force field of $Y_3N@C_{78}$ was used with Y atomic mass replaced by that of Dy. Raman intensities were computed numerically at the PBE0/6-31G level using PC GAMESS.[28]

Results and Discussion

The Most Stable Isomers of $M_3N@C_{78}$ (M = Sc, Y, La, Lu). At first, the isomers of C_{78} suitable for encapsulation of a metal−nitride cluster were determined. As the electronic

TABLE 1: Relative Energies (ΔE, kJ/mol) and HOMO−LUMO Gaps (gap, eV) of the Most Stable C_{78}^{6-} and $M_3N@C_{78}$ (M = Sc, Lu, Y, La) Isomers as Computed at DFT Level

cage	cage	C_{78}^{6-}		$Sc_3N@C_{78}$		$Lu_3N@C_{78}$		$Y_3N@C_{78}$		$La_3N@C_{78}$	
no[a]	symmetry	ΔE	gap	ΔE	gap	ΔE	gap	ΔE	gap	ΔE	gap
24 109	D_{3h}[b]	0.0	1.21	0.0	1.22	0.0	1.39	0.0	1.33	0.0	0.80
22 010	C_2	59.1	1.60	80.4	1.31	−61.8	1.52	−83.6	1.51	−157.7	1.53
24 107	C_{2v}[b]	96.7	0.60	91.5	0.58	89.9	0.54	83.4	0.55	68.6	0.48
22 646	C_1	110.3	1.22	137.6	1.13	0.8	1.28	−16.1	1.26	−108.8	1.15
24 088	C_{2v}	117.4	1.02	119.4	0.91	21.6	0.93	7.1	0.92	−25.8	0.91
21 975	C_1	120.0	1.27	137.5	1.05	3.7	1.28	−18.5	1.21	−104.8	1.07

[a] Numeration of C_{78} isomers is given in accordance with the spiral algorithm.[7] [b] IPR isomers; every other isomer in the table has two pairs of fused pentagons.

structure of trimetallic−nitride clusterfullerenes may be conceived as a result of a formal six-electron transfer from the cluster to the fullerene,[29] calculations of the empty cages were performed for the hexaanionic state. C_{78} has in total 24 109 isomers, and five of them conform with the IPR.[7] The isomers with three or more fused pentagons were avoided in this study because of the high-strain energy penalty in these geometries, reducing the number of isomers for AM1 level geometry optimization to 2927. Of these, the C_{78}^{6-} isomers most stable in the 300 kJ/mol range were subjected to point-energy computations at the DFT//AM1 level. Finally, complete DFT optimization was performed for the most stable structures within the 150 kJ/mol range. A perfect linear correlation between AM1 and DFT//AM1 relative energies was found (see Supporting Information Figure S1) thus justifying the use of semiempirical AM1 approach for the first exploratory search of the most stable isomers. Thus, only a limited set of the isomers found to be the most stable at the AM1 level may be further studied by much more computationally demanding DFT methods. The data for the six most stable structures are compiled in Table 1. The IPR isomer D_{3h}: 24 109, which was determined to be the cage of $Sc_3N@C_{78}$,[5b] was found to be the most stable isomer of C_{78}^{6-}. The second most stable isomer (relative energy 59.1 kJ/mol) is the non-IPR C_2: 22 010 cage, which contains two pairs of adjacent pentagons. Another IPR cage, C_{2v}: 24 107, is the third most stable (relative energy 96.7 kJ/mol), while the three other IPR cages have much higher relative energies.

DFT calculations revealed that encapsulation of the Sc_3N cluster in C_{78} does not change the order of relative stability found for hollow C_{78}^{6-}. $Sc_3N@C_{78}$ (D_{3h}: 24 109) is 80.4 kJ/mol more stable than the second most stable isomer, $Sc_3N@C_{78}$ (C_2: 22 010). However, upon replacing Sc_3N with larger clusters such as Lu_3N, Y_3N, or La_3N, the order of the relative stability has changed drastically. For these encaged clusters, the most stable isomer is the non-IPR C_2: 22 010 (Figure 3). Other isomers of $Y_3N@C_{78}$, $Lu_3N@C_{78}$, and $La_3N@C_{78}$ with non-IPR cages (C_1: 22 646, C_{2v}: 24 088, C_1: 21 975) are also significantly stabilized in comparison to IPR-obeying structures (Table 1).

The dramatic changes in the relative stabilities may be rationalized by the structures of the encaged clusters. While Sc_3N is planar in C_{78} (D_{3h}: 24 109),[5b] the limited space in this cage forces the larger clusters to be pyramidal (Figure 3, the calculated displacements of the nitrogen atom out of M_3 plane are 0.395 Å in Lu_3N, 0.554 Å in Y_3N, and 0.910 Å in La_3N). On the contrary, in the four lowest-energy non-IPR isomers, the cavity is large enough to accommodate Y_3N and Lu_3N clusters in a nearly or rigorously planar geometry. Although the La_3N cluster is too large to be planar in all C_{78} isomers studied, its pyramidalization in the most suitable non-IPR cages is less pronounced. Earlier, the low relative yield of $Gd_3N@C_{80}$ compared to $M_3N@C_{80}$ with smaller planar clusters such as

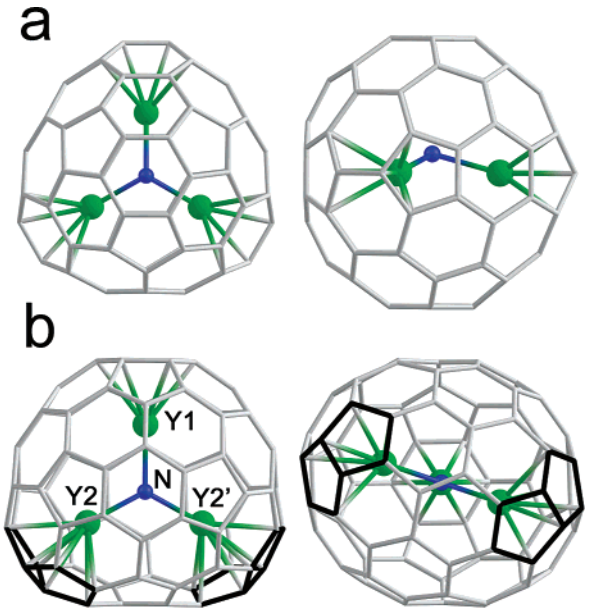

Figure 3. DFT-optimized structures of $Y_3N@C_{78}$: (a) isomer D_{3h}: 24 109; (b) isomer C_2: 22 010. Adjacent pentagons are highlighted in black. Selected distances (Å) and angles (°) for $Y_3N@C_{78}$ (C_2: 22 010): Y1−N, 2.072; Y2−N, 2.113; shortest Y1−C: 2.461, 2.452; shortest Y2−C: 2.481, 2.482, 2.496; Y1−N−Y2, 117.2; Y2−N−Y2′, 125.5.

Dy_3N was attributed to the pyramidalization of the larger Gd_3N cluster.[6a,26,30] Here, the pyramidalization of the clusters in the D_{3h}: 24 109 and C_2: 22 010 isomers of $M_3N@C_{78}$ (M = Sc, Y, Lu) provide quantified energy penalties of 142 kJ/mol for Lu_3N and 164 kJ/mol for Y_3N. Also, the destabilization of the $M_3N@C_{78}$ (D_{3h}: 24 109) isomer increases with the cluster size. While C_2: 22 010 is the only isomer of $Lu_3N@C_{78}$ which is more stable than D_{3h}: 24 109, $Y_3N@C_{78}$ and $La_3N@C_{78}$ have additional non-IPR isomers that are also more stable than the IPR-obeying structure (see Table 1).

Assignment of the Structure of $Tm_3N@C_{78}$ and $Dy_3N@C_{78}$ (II). The enhanced stability of $M_3N@C_{78}$ (C_2: 22 010) for metal ions with large radii makes this isomer the most probable one for the structure of the experimentally isolated $Tm_3N@C_{78}$ and $Dy_3N@C_{78}$ (II).[6] DFT computations for Dy_3N and Tm_3N clusterfullerenes are not feasible because of their partially filled f-shells, but assignment of the isomer is still possible. We have recently shown that the cluster−cage interactions as well as the spectroscopic properties of clusterfullerenes are largely determined by the ionic radii of the involved metal.[26] Since the ionic radius of Y (0.90 Å) is very close to that of Dy (0.91 Å) and only slightly larger than that of Tm (0.87 Å),[31] the structure and spectroscopic properties of $Y_3N@C_{78}$, $Dy_3N@C_{78}$, and $Tm_3N@C_{78}$ are assumed to be similar. Indeed, UV−vis−NIR, FTIR, and Raman spectra of $Dy_3N@C_{78}$ (II) and $Tm_3N@C_{78}$ are congruent (Figures 1, 2, 4, see below). Thus, the calculated

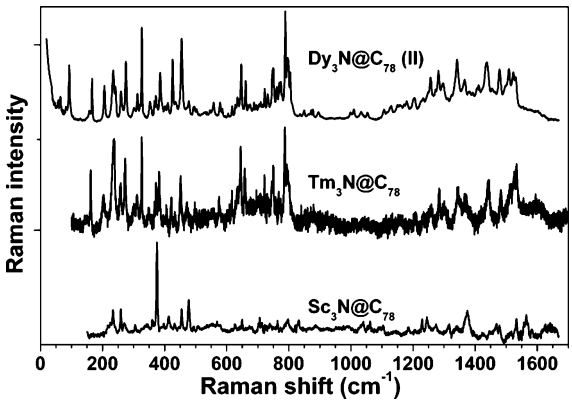

Figure 4. Raman spectra of $M_3N@C_{78}$ (M = Sc, Tm, Dy); excitation with 647.1 nm laser.

structure and spectra of $Y_3N@C_{78}$ are to a great extent transferable to the lanthanide-based clusterfullerenes.

The Y_3N cluster in DFT-optimized $Y_3N@C_{78}$ (C_2: 22 010) is planar and almost equilateral as illustrated in Figure 3. One of the yttrium atoms (Y1) faces the center of a hexagon, while two symmetry-related Y2 and Y2′ atoms are coordinated to the fused pentagons in a way similar to $Sc_3N@C_{68}$, $Sc_3N@C_{70}$, and $Tb_3N@C_{84}$,[4] thus stabilizing the pentagon junctions. The calculated HOMO−LUMO gap of $Y_3N@C_{78}$ (C_2: 22 010) is 1.51 eV, which is by 0.29 eV larger than the gap calculated for $Sc_3N@C_{78}$ (D_{3h}: 24 109, 1.22 eV). This larger calculated gap value corresponds to the experimental observation of the larger energies of HOMO−LUMO transitions in $Tm_3N@C_{78}$ (1.65 eV) and $Dy_3N@C_{78}$ (II) (1.67 eV) compared to the HOMO−LUMO transition in $Sc_3N@C_{78}$ (1.41 eV).

Vibrational Analysis of $Tm_3N@C_{78}$ and $Dy_3N@C_{78}$ (II). The most compelling arguments for the structural assignment of $Tm_3N@C_{78}$ and $Dy_3N@C_{78}$ (II) are based on the analysis of the vibrational spectra. The overall IR and Raman spectra of $Tm_3N@C_{78}$ and $Dy_3N@C_{78}$ (II) are shown in Figures 2 and 4 in comparison to those of $Sc_3N@C_{78}$ (D_{3h}: 24 109). The full list of vibrational wave numbers and relative intensities is provided in the Supporting Information. The vibrational structure of $Tm_3N@C_{78}$ and $Dy_3N@C_{78}$ (II) is characterized by the same dominating line groups in the IR and Raman spectra. The most intense infrared absorptions are observed in the tangential cage mode region from 1320 to 1400 cm^{-1}, where both spectra exhibit five strong or very strong, resolved lines. By analyzing the whole IR range, a nearly perfect one-to-one correspondence of IR lines can be found for $Tm_3N@C_{78}$ and $Dy_3N@C_{78}$ (II) with the exception of the two most intensive low-energy IR lines between 600 and 700 cm^{-1} which will be analyzed in detail below. Significant differences exist, on the other hand, in comparison to the infrared spectrum of $Sc_3N@C_{78}$ (D_{3h}: 24 109), which is extended far beyond 1500 cm^{-1}, has only three strong lines around 1350 cm^{-1}, no or only weak absorptions between 1000 and 1300 cm^{-1}, and no line at around 810 cm^{-1}. Similar conclusions are valid for the Raman spectra of $Tm_3N@C_{78}$ and $Dy_3N@C_{78}$ (II), for which also a one-to-one correspondence of lines can be established. The most pronounced characteristics in comparison to the Raman spectrum of $Sc_3N@C_{78}$ (D_{3h}: 24 109) are the low-energy line at around 160 cm^{-1}, the uniform Raman intensity in the lower radial cage mode region between 200 and 500 cm^{-1}, the higher Raman intensity in the higher radial cage mode region between 600 and 800 cm^{-1}, and the absence of lines above 1550 cm^{-1}.

Since the vibrational spectra of $Tm_3N@C_{78}$ and $Dy_3N@C_{78}$ (II) are so similar, the molecular structures should be based on the same carbon cage which is obviously not identical with that of $Sc_3N@C_{78}$ (D_{3h}: 24 109). Comparing the wave numbers of the related structures $Tm_3N@C_{78}$ and $Dy_3N@C_{78}$ (II) in detail, the former one has by up to 7 cm^{-1} higher frequencies in the tangential cage mode region. The latter one shows slightly higher wave numbers in the radial cage mode region, which are most pronounced for the $Dy_3N@C_{78}$ (II) lines at 426 cm^{-1} and 478 cm^{-1}, and their $Tm_3N@C_{78}$ counterparts at 421 and 473 cm^{-1}. Because of the much higher signal-to-noise ratio, the analysis of the vibrational spectra is given largely for $Dy_3N@C_{78}$ (II). In total, 151 lines were observed in the wave number range between 10 and 1700 cm^{-1}. From these lines, 60 were found in both the infrared and Raman spectrum, 19 were only infrared, and 72 were only Raman active.

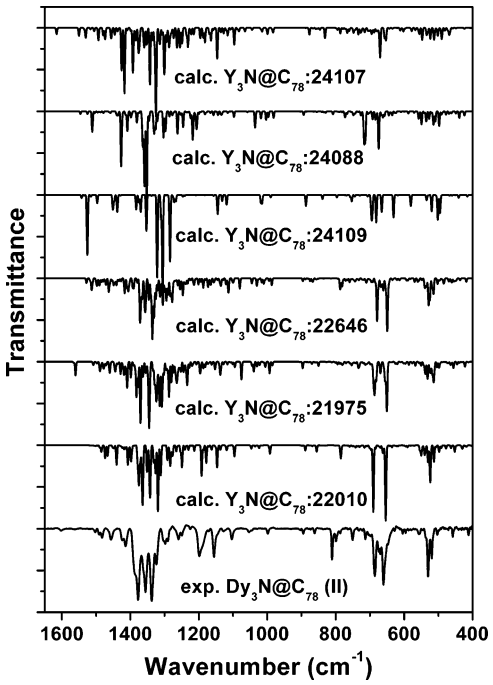

Figure 5. Experimental FTIR spectrum of $Dy_3N@C_{78}$ (II) compared to the calculated spectra for the low-energy isomers of $Y_3N@C_{78}$.

Figure 5 compares experimental FTIR spectrum of $Dy_3N@C_{78}$ (II) to the IR spectra calculated for the most stable isomers of $Y_3N@C_{78}$. The peak-to-peak agreement between experimental and computed spectra of C_2: 22 010 isomer is established in the whole frequency range, while computed spectra of other isomers of $Y_3N@C_{78}$ do not match the experimental one. The isomers 24 109, 24 088, and 24 107 have substantially different IR patterns, and their dissimilarity with the experimental data is obvious. Overall IR patterns for the isomers 21 975 and 22 646 are rather similar to that of 22 010, but peak-by-peak analysis of the experimental data in the vicinity of the tangential cage modes in comparison to the computed spectra shows that only the spectrum of the isomer 22 010 has a sufficient agreement (in terms of both frequencies and intensities) to provide unambiguous assignment for each experimental band. For instance, experimental IR bands (cm^{-1}) at 1103 (m), 1156 (s), 1199 (s), 1260 (m), 1290 (m), 1298 (m), 1304 (m), 1324 (s), 1338 (vs), 1356 (vs), 1364 (sh, s), 1377 (vs), 1388 (sh, s), 1414 (m), 1424 (m), and 1456 (m) are assigned to the calculated modes at 1095 (symmetry *B*, intensity 15% of the most intense mode), 1146 (*B*, 29%), 1191 (*B*, 36%), 1249 (*B*, 29%), 1276 (*B*, 13%), 1283 (*B*, 27%), 1291 (*B*, 19%), 1310 (*A*, 11%)/1312 (*B*, 28%), 1319 (*A*, 86%), 1341 (*B*, 57%), 1363 (*B*, 62%), 1375 (*B*, 53%), 1398 (*B*, 20%), 1407 (*B*, 26%), and 1440 (*B*, 23%), respectively (the systematic 10−15 cm^{-1} underestimation of the

computed frequencies is consistent with analogous downshifts in the earlier reported $Sc_3N@C_{78}$ and $Sc_3N@C_{68}$ clusterfullerenes[24]). Attempts to establish such correlations between experimental data and computed spectra of isomers 21 975 and 22 646 inevitably require either higher deviations of the computed frequencies from experimental wavenumbers or strong disagreement in the relative intensities.

While radial and tangential cage modes of $Dy_3N@C_{78}$ (II) are observed in the IR spectrum as medium intense lines in the 400−600 cm^{-1} range and medium to strong lines at 1000−1600 cm^{-1} ranges, respectively, the range of 600−700 cm^{-1} is dominated by the antisymmetric metal−nitrogen stretching modes. In C_3-symmetric $Dy_3N@C_{80}$ (I) clusterfullerene, this mode is 2-fold degenerated and appears at around 700−710 cm^{-1}.[26] As the cluster has only C_2 symmetry in $Dy_3N@C_{78}$ (22 010:C_2), the degeneracy of the ν_{as}(M−N) mode is lifted resulting in two intense lines at 661 and 685 cm^{-1} (641 and 682 cm^{-1} in $Tm_3N@C_{78}$). According to the calculations, the higher frequency line is due to the nitrogen atom displacements along the C_2 axis (i.e., presumably stretching of the shorter Y1−N bond), while $\perp C_2$ displacements (presumably stretching of the longer Y2−N and Y2′−N bonds) is assigned to the line at 661 cm^{-1}. The lower frequencies of these modes in comparison to $M_3N@C_{80}$ (I)[26] are in line with the longer Y−N bond lengths predicted by DFT calculations in $Y_3N@C_{78}$ (Y1−N, 2.072 Å; Y2−N, 2.113 Å) as compared to $Y_3N@C_{80}$ (2.060 Å).

Raman excitation wavelengths (514.5 and 647.1 nm) used in this work match the absorption range of $Dy_3N@C_{78}$ (II), and the intensity of the totally symmetric modes is expected to be enhanced because of the resonance Raman scattering conditions. This fact considerably complicates the assignment of the spectra, since the experimental Raman spectra exhibit an intensity distribution different from the calculated one for off-resonance Raman scattering conditions. Analogous lack of coincidence between the computed off-resonance Raman intensities and experimental resonance Raman data was reported earlier for $Sc_3N@C_{68}$ and $Sc_3N@C_{78}$ and is the subject of further computational efforts.[24] Since the vibrational density of states for $Dy_3N@C_{78}$ (II) tangential and high-energy radial cage modes is too high to allow a reliable assignment on the basis only of the computed wave numbers, the analysis is focused on the less crowded low-frequency range, which is of particular value for the clarification of structural details of endohedral clusterfullerenes, since (1) the metal cage modes directly reflect the nature and the strength of the M_3N-cage bond[15b,26] and (2) the splitting of the so-called squashing mode is a measure for the ratio of the three main moments of inertia and therefore for the deviation of the probed carbon cage from a spherical shape.[32] Figure 6 displays the line shape analysis for the low-energy Raman spectra of $Dy_3N@C_{78}$ (II) measured with two different laser lines. Computed spectrum provides reasonable agreement with the experimental data once resonance enhancement of the intensities of the *A*-symmetry modes at 92, 166, and 275 cm^{-1} is taken into account.

The achieved agreement allows the full assignment of metal-based modes of $M_3N@C_{78}$. The vibrational representation of a M_3N cluster with idealized D_{3h} symmetry has the following form in a C_2-symmetric environment:

$$\Gamma_{vib}(M_3N, D_{3h} \rightarrow C_2) = 1A_1' (\rightarrow A: \nu_s) + 1A_2' (\rightarrow B: R_z) + 2A_2'' (\rightarrow B: \gamma, T_z) + 3E' (\rightarrow A: T_x, \nu_{as}, \delta + B: T_y, \nu_{as}, \delta) + 1E'' (\rightarrow A: R_x + B: R_y)$$

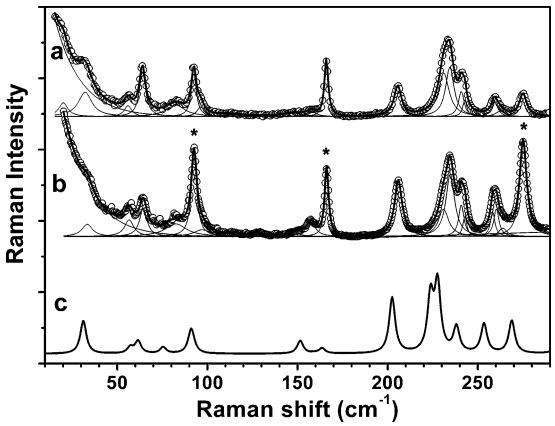

Figure 6. Low-energy part of Raman spectra of $Dy_3N@C_{78}$ (II) with line-shape analysis: (a) excitation with 514.5 nm laser; (b) excitation with 647.1 nm laser; (c) calculated for off-resonance conditions. The asterisks mark *A*-symmetry bands whose intensities are enhanced presumably because of the resonance conditions.

where *x* and *y* axes lie in plane of the M_3N cluster and are chosen to be along and perpendicular to the C_2 axis. Among the 11 Raman lines found below 180 cm^{-1}, 8 are in excellent agreement with the cluster−cage modes or the cluster modes found by the computation (see Table 2). From the three remaining lines, the lowest energetic one at 20 cm^{-1} is assigned to a lattice mode, and two very weak lines at 128 and 149 cm^{-1} are tentatively attributed to overtones (twofold wave number of the fundamental at 64 cm^{-1} and a combination of 57 cm^{-1} + 93 cm^{-1}). Frustrated rotations of the cluster are assigned to the low-energy bands at 32 (sh, m, R_y), 57 (w, R_z), and 64 cm^{-1} (m, R_x). The weak feature at 82 cm^{-1} is due to the cluster displacement perpendicular to its bonding plane. The strong line at 92 cm^{-1} can be assigned to the totally symmetric Y2−N−Y2′ bending mode, while its antisymmetric counterpart (i.e., Y1−N−Y2 bending) is found as a shoulder at 96 cm^{-1} with much lower intensity. The mode with a predominant contribution of the T_y displacement appears at 157 cm^{-1} (w), while the *A*-symmetric frustrated translation along C_2 axis of the molecule appears as a strong line at 166 cm^{-1}. From the cluster modes expected in this frequency range, only $\gamma(Dy_3N)$ (i.e., the out-of-plane motion of nitrogen atom) expected at 154 cm^{-1} (calcd) could not be found in the experimental spectrum presumably because of the low Raman intensity.

The range of 200−300 cm^{-1} includes the totally symmetric metal−nitrogen stretching vibration ν_s(M−N) and the squashing mode of the carbon cage (analogous to the $H_g(1)$ squashing mode of C_{60} at 270 cm^{-1}), which is split into $3A + 2B$ irreducible representations in C_2 symmetry group. Potential energy distribution analysis has shown that ν_s(M−N) is mixed with two *A*-symmetric components of the squashing mode, and these complex vibrations can be ascribed to the medium intense lines at 206 cm^{-1} and 241 cm^{-1}. The squashing mode splitting (206−275 cm^{-1}) points to a strong deviation from spherical shape of the molecule, which is in line with the proposed C_2: 22 010 structure of $Dy_3N@C_{78}$ (II).

Noteworthily, the observation of totally 11 fundamental IR and Raman modes of Dy_3N cluster as well as the total amount of observed IR and Raman lines directly point to a molecular symmetry without degenerated and dipole-forbidden irreducible representations, that is, at maximum C_2 or C_s.

The breathing mode (BM) of the carbon cage can be presumably assigned to the very strong line at 454 cm^{-1} (calcd 445 cm^{-1}). Eisler et al.[32a] has shown that the frequency of the breathing mode is almost independent of the cage shape and is

TABLE 2: Cluster Modes in $Dy_3N@C_{78}$ (II) Calculated at the DFT Level and Observed in the Experimental Spectra

symmetry	frequency	I(IR)[a]	exptl	IR	I(ram)[a]	exptl ram	514.5 nm	exptl ram	647 nm	assignment[b]
B	30.9	2.1			43.3	32	sh, m	33	sh	R_y
B	57.5	2.7			8.0	56	w	57	w	R_z
A	61.3	0.7			16.2	64	m	64	m	R_x
B	75.7	9.3			8.4	82	w	82	w	T_z
A	91.0	2.7			30.3	92	m	93	s	δ(Y2−N−Y2)
B	92.2	9.1			3.7	96	sh	97	sh	δ(Y1−N−Y2)
B	151.5	1.5			16.9			157	w	T_y
B	159.3	10.4			0.9					$\gamma(Dy_3N)$
A	163.6	1.1			6.9	166	m	166	s	T_x
A	202.5	0.0			73.2	206	w	206	m	$\nu_{s,Dy-N} + C_{78}$ (63%)[c]
A	238.1	0.1			33.7	241	s	241	m	$\nu_{s,Dy-N} + C_{78}$ (54%)[c]
B	647.7	100.0	661	vs	1.1					$\nu_{as,Dy-N}$ (N displ. $\perp C_2$)
A	683.1	80.1	685	vs	0.6	687	w	688	w	$\nu_{as,Dy-N}$ (N displ. $\parallel C_2$)

[a] Computed intensities are given in % with respect to the most intense lines. [b] T, translation; R, rotation; δ, Y−N−Y bending; γ, nitrogen out-of-plane displacement; ν_s and ν_{as}, symmetric and antisymmetric Dy−N stretching vibrations. [c] As the cluster vibration is mixed with the cage mode, the cage contribution to the potential energy is given in parentheses.

primarily determined by the root of the inverse mass. The BM frequency in $Dy_3N@C_{78}$ (II) is ca. 20 cm^{-1} higher compared to the isomers of hollow C_{78} (430 cm^{-1} in D_3, 429 cm^{-1} in C_{2v}, 434 cm^{-1} in C_{2v}')[32a] and is close to the frequency of the BM in C_{70} (455 cm^{-1}). Such a hardening of BM in $Dy_3N@C_{78}$ (II) compared to the hollow fullerenes of the same cage mass can be readily explained by stiffening of the cage caused by the covalent cluster−cage interactions.

Conclusions

DFT computations in combination with an FTIR and Raman analysis have demonstrated the role of the cluster size for the fullerene cage isomerism in trimetallic nitride clusterfullerenes for the first time. Destabilization caused by the pyramidalization of the trimetallic nitride clusters was quantified as 140−160 kJ/mol. For C_{78}, this value is sufficient to change the isomer stability order of the $M_3N@C_{78}$ clusterfullerenes upon replacing Sc_3N by larger clusters. The non-IPR C_2: 22 010 isomer of C_{78} is the lowest energy isomer with a suitable cavity to host planar lanthanide-based M_3N clusters, and this structure is assigned to the experimentally isolated $Tm_3N@C_{78}$ and $Dy_3N@C_{78}$ (II).[33]

The structural assignment based on the energetic considerations is further solidified by vibrational spectroscopic studies. While DFT computed spectra of other low-energy isomers of $Y_3N@C_{78}$ do not match the experimental data for $Dy_3N@C_{78}$ (II) and $Tm_3N@C_{78}$, IR and Raman spectra of the non-IPR C_2: 22 010 isomer of $Y_3N@C_{78}$ perfectly match the measured data, enabling us to propose a detailed vibrational assignment for $Dy_3N@C_{78}$ (II) and $Tm_3N@C_{78}$. This study shows that vibrational spectroscopy supplemented with reliable theoretical modeling can provide a powerful tool in the structural research of endohedral fullerenes when X-ray or NMR does not provide unambiguous solutions to the problem or fails because of low amounts of the fullerene structure under study.

Acknowledgment. This work was supported by CRDF (A. A. P., award RUC2-2830-MO-06), DAAD (A. A. P., J. W.), and Alexander von Humboldt Foundation (S. Y.). We thank Prof. Chun-Ru Wang (Institute of Chemistry, CAS, Beijing) for the program used to generate fullerene isomers.

Supporting Information Available: Relative energies and HOMO−LUMO gaps of the most stable C_{78}^{6-} isomers, correlation between AM1 and DFT relative energies, DFT-optimized Cartesian coordinates of $Y_3N@C_{78}$ isomers listed in Table 1, the list of all experimentally observed IR and Raman bands, calculated frequencies and intensities of $Dy_3N@C_{78}$ (II).[34] This material is available free of charge via the Internet at http://pubs.acs.org.

References and Notes

(1) (a) Akasaka, T.; Nagase S. *Endofullerenes: A New Family of Carbon Cluster*: Kluwer Academic Publishers: Dordrecht, 2002. (b) Dunsch, L.; Yang, S. *Electrochem. Soc. Interface* **2006**, *15* (2), 34−39.

(2) (a) Kobayashi, K.; Nagase, S. *Chem. Phys. Lett.* **1997**, *274*, 226−230. (b) Seifert, G.; Bartl, A.; Dunsch, L.; Ayuela, A.; Rockenbauer, A. *Appl. Phys. A* **1998**, *66*, 265−271.

(3) (a) Wang, C. R.; Kai, T.; Tomiyama, T.; Yoshida, T.; Kobayashi, Y.; Nishibori, E.; Takata, M.; Sakata, M.; Shinohara, H. *Nature* **2000**, *408*, 426−427. (b) Kato, H.; Taninaka, A.; Sugai, T.; Shinohara, H. *J. Am. Chem. Soc.* **2003**, *125*, 7782−7783. (c) Shi, Z. Q.; Wu, X.; Wang, C. R.; Lu, X.; Shinohara, H. *Angew. Chem., Int. Ed.* **2006**, *45*, 2107−2111. (d) Wakahara, T.; Nikawa, H.; Kikuchi, T.; Nakahodo, T.; Rahman, G. M. A.; Tsuchiya, T.; Maeda, Y.; Akasaka, T.; Yoza, K.; Horn, E.; Yamamoto, K.; Mizorogi, N.; Slanina, Z.; Nagase, S. *J. Am. Chem. Soc.* **2006**, *128*, 14228−14229.

(4) (a) Stevenson, S.; Fowler, P. W.; Heine, T.; Duchamp, J. C.; Rice, G.; Glass, T.; Harich, K.; Hajdu, E.; Bible, R.; Dorn, H. C. *Nature* **2000**, *408*, 427−428. (b) Yang, S.; Popov, A. A.; Dunsch, L. *Angew. Chem., Int. Ed.* **2007**, *46*, 1256−1259. (c) Beavers, C. M.; Zuo, T.; Duchamp, J. C.; Harich, K.; Dorn, H. C.; Olmstead, M. M.; Balch, A. L. *J. Am. Chem. Soc.* **2006**, *128*, 11352−11353.

(5) (a) Stevenson, S.; Rice, G.; Glass, T.; Harich, K.; Cromer, F.; Jordan, M. R.; Craft, J.; Hajdu, E.; Bible, R.; Olmstead, M. M.; Maitra, K.; Fisher, A. J.; Balch, A. L.; Dorn, H. C. *Nature* **1999**, *401*, 55−57. (b) Olmstead, M. M.; Bettencourt-Dias, A.; Duchamp, J. C.; Stevenson, S.; Marciu, D.; Dorn, H. C.; Balch, A. L. *Angew. Chem., Int. Ed.* **2001**, *40*, 1223−1225. (c) Dunsch, L.; Krause, M.; Noack, J.; Georgi, P. *J. Phys. Chem. Solids* **2004**, *65*, 309−315. (d) Stevenson, S.; Lee, H. M.; Olmstead, M. M.; Kozikowski, C.; Stevenson, P.; Balch, A. L. *Chem. Eur. J.* **2002**, *8*, 4528−4535.

(6) (a) Krause, M.; Dunsch, L. *Angew. Chem., Int. Ed.* **2005**, *44*, 1557−1560. (b) Krause, M.; Wong, J.; Dunsch, L. *Chem. Eur. J.* **2005**, *11*, 706−711. (c) Yang, S.; Dunsch, L. *J. Phys. Chem. B* **2005**, *109*, 12320−12328.

(7) Fowler, P. W.; Manolopoulos, D. E. *An Atlas of Fullerenes:* Clarendon Press: Oxford, U.K., 1995.

(8) Campanera, J. M.; Bo, C.; Poblet, J. M. *Angew. Chem., Int. Ed.* **2005**, *44*, 7230−7233.

(9) (a) Schettino, V.; Pagliai, M.; Ciabini, L.; Cardini, G. *J. Phys. Chem. A* **2001**, *105*, 11192−11196. (b) Menendez, J.; Page, J. B. Light Scattering in Solids VIII. In *Topics in Applied Physics*; Cardona, M.; Güntherodt, G., Eds.; Springer-Verlag: Berlin Heidelberg, 2000; pp 27−95.

(10) Schettino, V.; Pagliai, M.; Cardini, G. *J. Phys. Chem. A* **2002**, *106*, 1815−1823 and refs therein.

(11) Bettinger, H. F.; Scuseria, G. E. *Chem. Phys. Lett.* **2000**, *332*, 35−42.

(12) Kuzmany, H.; Plank, W.; Winter, J.; Dubay, O.; Tagmatarchis, N.; Prassides, K. *Phys. Rev. B* **1999**, *60*, 1005−1012.

(13) Bini, R.; Ebenhoch, J.; Fanti, M.; Fowler, P. W.; Leach, S.; Orlandi, G.; Rüchardt, Ch.; Sandall, J. P. B.; Zerbetto, F. *Chem. Phys.* **1998**, *232*, 75−94.

(14) (a) Long, V. C.; Musfeldt, J. L.; Kamaras, K.; Adams, G. B.; Page, J. B.; Iwasa, Y.; Mayo, W. E. *Phys. Rev. B* **2000**, *61*, 13191. (b) Zhu, Z.-T.; Musfeldt, J. L.; Kamaras, K.; Adams, G. B.; Page, J. B.; Kashevarova, L. S.; Rakhmanina, A. V.; Davydov, V. A. *Phys. Rev. B* **2002**, *65*, 085413.

(c) Zhu, Z.-T.; Musfeldt, J. L.; Kamaras, K.; Adams, G. B.; Page, J. B.; Kashevarova, L. S.; Rakhmanina, A. V.; Davydov, V. A. *Phys. Rev. B* **2003**, *67*, 045409.

(15) (a) Krause, M.; Hulman, M.; Kuzmany, H.; Dennis, T. J. S.; Inakuma, M.; Shinohara, H. *J. Chem. Phys.* **1999**, *111*, 7976−7984. (b) Krause, M.; Kuzmany, H.; Georgi, P.; Dunsch, L.; Vietze, K.; Seifert, G. *J. Chem. Phys.* **2001**, *115*, 6596−6605. (c) Kobayashi, K.; Nagase, S. *Mol. Phys.* **2003**, *101*, 249−254. (d) Shimotani, H.; Ito, T.; Iwasa, Y. T., A.; Shinohara, H.; Nishibori, E.; Takata, M.; Sakata, M. *J. Am. Chem. Soc.* **2004**, *126*, 364−369.

(16) Laikov, D. N. *Chem. Phys. Lett.* **1997**, *281*, 151−6.

(17) Perdew, J. P.; Burke, K.; Ernzerhof, M. *Phys. Rev. Lett.* **1996**, *77* (18), 3865−3868.

(18) (a) Senyavin, V. M.; Popov, A. A.; Granovsky, A. A.; Davydov, V. A.; Agafonov, V. N. *Fullerenes, Nanotubes, Carbon Nanostruct.* **2004**, *12*, 253−258. (b) Senyavin, V. M.; Popov, A. A.; Granovsky, A. A. In *Hydrogen Materials Science and Chemistry of Carbon Nanomaterials*; Veziroglu, T. N., Zaginaichenko, S. Yu.; Schur, D. V.; Baranowski, B.; Shpak, A. P., Skorokhod, V. V., Eds.; NATO Science Series II: Mathematics, Physics and Chemistry: 2004; Vol. 172, pp 457−465.

(19) Popov, A. A.; Senyavin, V. M.; Granovsky, A. A.; Lobach, A. S. In *Hydrogen Materials Science and Chemistry of Carbon Nanomaterials*; Veziroglu, T. N.; et al., Eds.; NATO Science Series II: Mathematics, Physics and Chemistry: 2004; 172, pp 347−356.

(20) (a) Popov, A. A.; Senyavin, V. M.; Granovskii, A. A. *Chem. Phys. Lett.* **2004**, *383*, 149−155. (b) Popov, A. A.; Senyavin, V. M.; Granovsky, A. A. *Fullerenes, Nanotubes, Carbon Nanostruct.* **2004**, *12*, 305−310.

(21) (a) Denisenko, N. I.; Popov, A. A.; Kouvitchko, I. V.; Boltalina, O. V.; Chelovskaya. N. V. In *The exciting world of Nanocages and Nanotubes*; Kamat, P., Guldi, D., Kadish, K., Eds.; Fullerenes, Vol. 12; The Electrochemical Society: Pennington, NJ, 2002; pp 577−586. (b) Troyanov, S. I.; Denisenko, N. I.; Popov, A. A.; Boltalina, O. V.; Kemnitz, E. *Angew. Chem., Int. Ed.* **2003**, *42*, 2395.

(22) (a) Kuvychko, I. V.; Streletskii, A. V.; Popov, A. A.; Kotsiris, S. G.; Drewello, T.; Strauss, S. H.; Boltalina, O. V. *Chem. Eur. J.* **2005**, *11*, 5426−5436. (b) Popov, A. A.; Senyavin, V. M.; Troyanov, S. I. *J. Phys. Chem. A* **2006**, *110*, 7414−7421.

(23) (a) Popov, A. A.; Goryunkov, A. A.; Goldt, I. V.; Kareev, I. E.; Kuvychko, I. V.; Hunnius, W. D.; Seppelt, K.; Strauss, S. H.; Boltalina, O. V. *J. Phys. Chem. A* **2004**, *108*, 11449−11456. (b) Denisenko, N. I.; Troyanov, S. I.; Popov, A. A.; Kuvychko, I. V.; Zemva, B.; Kemnitz, E.; Strauss, S. H.; Boltalina, O. V. *J. Am. Chem. Soc.* **2004**, *126*, 1618−1619. (c) Popov, A. A.; Senyavin, V. M.; Boltalina, O. V.; Seppelt, K.; Spandl, J.; Feigerle, C. S.; Compton, R. N. *J. Phys. Chem. A* **2006**, *110*, 8645−8652.

(24) (a) Yang, S.; Kalbac, M.; Popov, A.; Dunsch, L. *Chem. Eur. J.* **2006**, *12*, 7856−7863. (b) Krause, M.; Popov, A.; Dunsch, L. *Chem. Phys. Chem.* **2006**, *7*, 1734−1740.

(25) Yang, S.; Kalbac, M.; Popov, A.; Dunsch. L. *Chem. Phys. Chem.* **2006**, *7*, 1990−1995.

(26) Yang, S.; Troyanov, S. I.; Popov, A. A.; Krause, M.; Dunsch, L. *J. Am. Chem. Soc.* **2007**, *128*, 16733−16739.

(27) Dewar, M.; Thiel, W. *J. Am. Chem. Soc.* **1977**, *99*, 4499.

(28) Granovsky, A. A. PC GAMESS version 7.0, 2006, http://classic-.chem.msu.su/gran/gamess/index.html.

(29) (a) Alvarez, L.; Pichler, T.; Georgi, P.; Schwieger, T.; Peisert, H.; Dunsch, L.; Hu, Z.; Knupfer, M.; Fink, J.; Bressler, P.; Mast, M. S.; Golden. *Phys. Rev. B* **2002**, *66*, 035107-1-7. (b) Campanera, J. M.; Bo, C.; Olmstead, M. M.; Balch, A. L.; Poblet, J. M. *J. Phys. Chem. A* **2002**, *106*, 12356−12364.

(30) Stevensen, S.; Phillips, J. P.; Reid, J. E.; Olmstead, M. M.; Rath, S. P.; Balch, A. L. *Chem. Commun.* **2005**, 2814−2815.

(31) Greenwood, N. N.; Earnshaw, A. *Chemistry of the Elements*; Pergamon: Oxford, U.K., 1984.

(32) (a) Eisler, H.-J.; Gilb, S.; Hennrich, F. H.; Kappes, M. M. *J. Phys. Chem. A* **2000**, *104*, 1762−1768. (b) Eisler, H.-J.; Hennrich, F. H.; Gilb, S.; Kappes, M. M. *J. Phys. Chem. A* **2000**, *104*, 1769−1773.

(33) Isolated amounts of the minor $Dy_3N@C_{78}$ (I) isomer[6c] are not sufficient yet for vibrational spectroscopic characterization, but its vis−NIR spectrum (Figure 1) clearly shows that its cage structure is also different from $Sc_3N@C_{78}$. On the basis of the stability and HOMO−LUMO gap, we may tentatively propose that $Dy_3N@C_{78}$ (I) is a non-IPR clusterfullerene with either C_1: 22 646 or C_1: 21 975 cage structure.

(34) A complete list of AM1 energies and coordinates for 2927 isomers of C_{78}^{6-} is available from A.A.P. upon request.